

<https://doi.org/10.1038/s43247-023-00734-4>

OPEN

## The mean state of the tropical Pacific Ocean differed between the Medieval Warm Period and the Industrial Era

Shiwei Jiang<sup>1</sup>, Xin Zhou<sup>1✉</sup>, Julian P. Sachs<sup>2</sup>, Zhibo Li<sup>3</sup>, Luyao Tu<sup>4</sup>, Yiyi Lin<sup>1</sup>, Xuanqiao Liu<sup>1</sup>, Anze Chen<sup>1</sup> & Yanan Shen<sup>1</sup>

Changes in the El Niño Southern Oscillation over the last few decades have been linked to anthropogenic greenhouse gas emissions; however, the sign, magnitude, and drivers of these variations during the Common Era are not yet well constrained. Here, we present an 1800-year reconstruction of the El Niño Southern Oscillation mean-state derived from precipitation reconstructions based on lake sediments in East Asia and examine the long-term changes in the mean state and variance of the tropical Pacific. We find that the Medieval Warm Period was characterized by La Niña-like states with low variance, whereas El Niño-like states prevailed during the Little Ice Age and the Current Warm Period with high variance. Temperature changes caused by effective radiative forcing were probably the drivers of this response during the pre-industrial period, whereas greenhouse gas forcing likely accounts for the variations in the tropical Pacific mean-state during the industrial period.

<sup>1</sup>School of Earth and Space Sciences, University of Science and Technology of China, Hefei 230026, China. <sup>2</sup>School of Oceanography, University of Washington, Seattle 98195, USA. <sup>3</sup>Laboratory for Climate and Atmosphere-Ocean Studies, Department of Atmospheric and Oceanic Sciences, School of Physics, Peking University, Beijing 100029, China. <sup>4</sup>School of Marine Science and Engineering, Nanjing Normal University, Nanjing 210046, China. ✉email: [xinzhou@ustc.edu.cn](mailto:xinzhou@ustc.edu.cn)

The El Niño–Southern Oscillation (ENSO) is characterized by a seesaw pattern of SST and atmospheric pressure between the eastern and western tropical Pacific that influences climate across the globe through atmospheric teleconnections<sup>1–3</sup>. The responses of ENSO variations to tropical Pacific mean-states under increased greenhouse gases are not yet well constrained<sup>4–6</sup>. Understanding the natural variability of ENSO and its responses to different tropical Pacific climatic mean states in the pre-industrial period are essential for validating climate models and predicting its future behavior under global warming<sup>7,8</sup>.

Tropical Pacific observational data, covering only about the past 150 years, are too short to allow for the investigation of the long-term changes in mean state, which further limits how we can explore the relationship between ENSO variability and mean states. Paleoclimate datasets and climate models provide insights to determine the characteristics of the mean state. Southern Oscillation Index (SOI) reconstructions, sea surface temperature (SST) records in the central or eastern Pacific, and zonal SST gradients across the tropical Pacific are often used as benchmarks for the tropical Pacific mean state over the past millennium<sup>9–16</sup>. Negative (positive) SOI, warmer (cooler) eastern Pacific SSTs, and a decreased (enhanced) zonal SST gradient on interdecadal and centennial time scales indicate an El Niño-like (La Niña-like) state (collectively referred to in this study as the mean state of the tropical Pacific). To date, changes in the mean state of the tropical Pacific in the pre-instrumental period have been reconstructed mostly from SST records and/or the oxygen isotope composition of corals and surface-dwelling foraminifera in the western, central, and eastern Pacific Ocean<sup>9–14</sup>. They indicate that La Niña-like conditions were more common during the Medieval Warm Period (MWP; ~1000–1300 CE), as compared to the Little Ice Age (LIA; ~1400–1850 CE) when El Niño-like conditions were more common. Yet, according to climate models even small El Niño-related tropical SST anomalies that are undetected by paleotemperature proxies can lead to discernible local precipitation anomalies<sup>17</sup>. Therefore, alternative hydrological records in the equatorial Pacific region<sup>15,18</sup> have been used to reconstruct past SOI to explore changes in mean state<sup>16</sup>. In contrast to SST-inferred changes in mean states, the SOI reconstruction based on hydroclimate reconstructions indicates a prevalence of El Niño-like states during the MWP and La Niña-like states during the LIA<sup>16</sup>. Climate model simulations also yield contradictory changes in mean states during the last millennium<sup>12,19,20</sup>. To reconcile these opposing views of last-millennium changes in mean state it is argued that precipitation changes in the tropical Pacific are influenced by both meridional movements of the Intertropical Convergence Zone (ITCZ) and zonal changes in the Pacific Walker Circulation (PWC)<sup>18,21–23</sup>, complicating their use as a strict indicator of the mean state of the tropical Pacific.

Given the lingering debate amongst climate researchers about natural changes in the tropical Pacific mean-state during the two largest climate perturbations (the MWP and the LIA) of the last millennium, there is a clear need for additional mean state reconstructions, particularly hydroclimate records that are not influenced by ITCZ variations that may occur in the absence of changes in mean state. The East Asian region, particularly eastern China, is outside the direct influence of the ITCZ. A strong teleconnection between precipitation in East Asia and SST anomalies has been previously established, with changes of SST patterns in the eastern equatorial Pacific (i.e., the mean state of the tropical Pacific) associated with coherent rainfall changes in East Asia on interdecadal<sup>24</sup>, centennial<sup>22,23,25,26</sup>, and millennial timescales<sup>27,28</sup>. Specifically, observational data showed that a decrease (increase) of average summer precipitation in the Jiang-Huai (JH) region (North China (NC) region) that temporally

coincided with the La Niña-like state (i.e., positive SOI) that prevailed from 1951 to 1978 CE, and increased (decreased) precipitation in the JH region (NC region) from 1979 to 1992 CE that coincided with the El Niño-like state during that time (i.e., negative SOI) (Fig. S1). Likewise, a decrease (increase) of precipitation in the JH (NC) region was found to coincide with the La Niña-like states of the tropical Pacific that prevailed during the MWP and mid-Holocene<sup>26–28</sup>. The unique location and teleconnection to the tropical Pacific make hydroclimate reconstructions from the East Asian region well suited for reconstructing the mean state of the tropical Pacific.

Precipitation changes in the JH region tend to be opposite those in the NC region and are closely related to the mean state of the tropical Pacific (Fig. 1; Supplementary Table S1). We utilized precipitation reconstructions from Lake Nvshan (in JH region) and Lake Gonghai (in NC region) to produce an 1800-year index of the tropical Pacific mean-state that is compared to global mean temperature (GMT) reconstructions to decipher causal mechanisms responsible for the changes in the mean state that could be linked to effective solar irradiance and greenhouse gas concentrations. The results provide new insights into changes in mean state and their forcing on centennial timescales over the past millennium, and contribute to an improved understanding of the response of tropical Pacific variability to different mean states.

## Results and discussion

**Spatial modes of precipitation in East Asia linked to tropical Pacific SSTs.** Twenty precipitation reconstructions from East Asia that span the last millennium were divided into two types according to the classification method of dry-wet grades<sup>23</sup> (Fig. 1). Most precipitation records from the JH region show enhanced (diminished) precipitation during the LIA (MWP) (Fig. S2). In contrast, most precipitation records from the NC region and the South China (SC) region indicate diminished (enhanced) precipitation during the LIA (MWP) (Figs. S3 and S4). The LIA (~1400–1850 CE) was characterized by Northern Hemisphere temperatures about 0.5 °C cooler than the mean temperature during the instrumental period (1961–1990 CE)<sup>12,29,30</sup>. The MWP (~1000–1300 CE) was the most recent pre-industrial era warm interval and was characterized by Northern Hemisphere temperatures close to the mean temperature during the instrumental period (1961–1990 CE)<sup>12,29,30</sup>. Both periods are thought to have been forced by combinations of solar irradiance, volcanic activity, greenhouse gases, and land use changes<sup>19,31–33</sup>. Previous studies have found significant hydroclimatic anomalies on both regional and global scales during these two periods<sup>21,34–37</sup>. Furthermore, the JH region was characterized by a “warm-dry, cool-wet” condition, while the NC region was characterized by a “warm-wet, cool-dry” condition during the last millennium<sup>26</sup>. The spatial pattern of centennial summer precipitation variability in East Asia shows a tripole “dry-wet-dry” pattern during the LIA and a “wet-dry-wet” pattern during the MWP<sup>26</sup> (Fig. S5). This is the same precipitation tripole pattern that occurred during El Niño-like state from the instrumental period (Fig. 1).

Previous studies reveal a close relationship between precipitation variations in East Asia and tropical Pacific SST patterns over the past millennium that are attributed to the systematic changes in the zonal atmospheric circulation<sup>25–28,38</sup>. Enhanced precipitation in the JH region and diminished precipitation in the NC region significantly modulated by eastern tropical Pacific SST anomalies (i.e., El Niño-like) as demonstrated by observational data<sup>24</sup>, paleoclimate datasets<sup>25–28</sup>, and climate models<sup>38–41</sup>. Ascending motion over the eastern tropical Pacific caused by warm SST anomalies induce anticyclonic motion and subsidence over the western tropical Pacific region<sup>38</sup>. This process

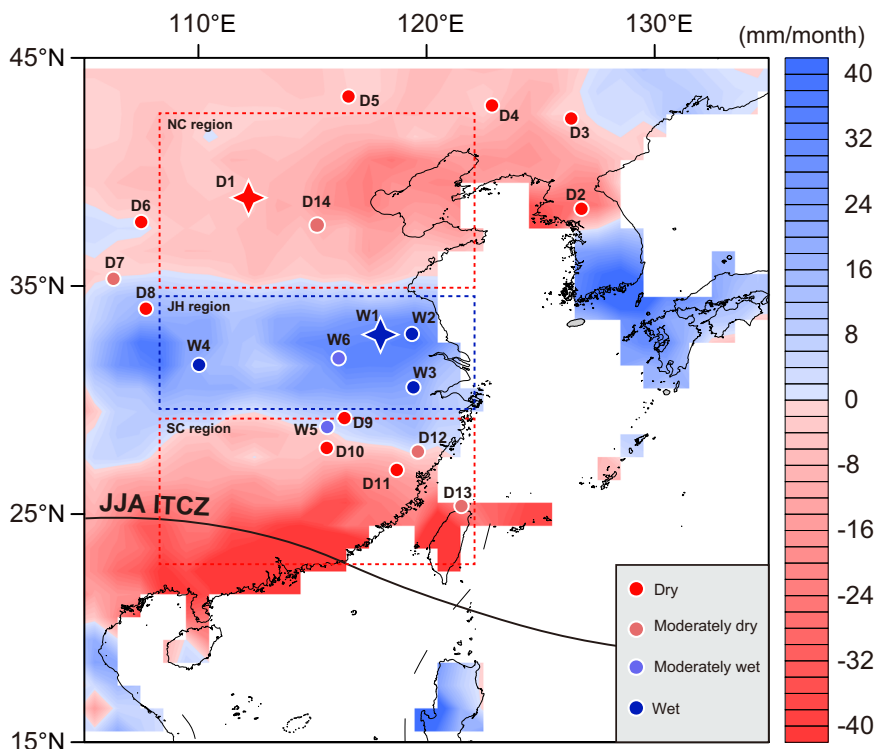


**Fig. 1 Map of June-August precipitation anomalies during El Niño-like state in East Asia with the locations of last millennium precipitation reconstructions used in this study.** Locations that were wetter during the LIA than during the MWP are indicated by blue symbols, while those that were drier during the LIA than during the MWP are indicated by red symbols. The stars denote the precipitation records used for reconstruction of the index of the tropical Pacific mean-state in this study (see Supplementary Table S1). Background shading shows the empirical orthogonal function mode 1 (EOF1) of instrumental (GPCP) summer (June-August, JJA) precipitation anomalies over East Asia during the 17 ENSO events that occurred between 1960–2020 CE (same as an El Niño-like state), which indicated an increase (decrease) of summer precipitation in the JH region (NC region) under an El Niño-like state. That areas with positive precipitation anomalies are shaded in blue, while those with negative precipitation anomalies are shaded in red. The dashed rectangular boxes indicate the tripole pattern of precipitation anomalies in East Asia that are the basis for reconstructing the mean state of the tropical Pacific from East Asian JJA precipitation records.

strengthens the Western Pacific Subtropical High (WPSH) and results in more water vapor within the JH region, and less water vapor within the NC region. The simulation results show that a weaker (eastward) WPSH occurred during the MWP and a stronger (westward) WPSH occurred during the LIA<sup>42</sup>, which support the interpretation that the precipitation in eastern China is linked to the mean state of the tropical Pacific via a teleconnection involving the WPSH. Modern observational data also support this teleconnection between East Asia and the tropical Pacific (Fig. S6). A persistent La Niña-like state from ~1960 to 1980 CE was associated with a weaker WPSH and diminished (enhanced) precipitation in the JH (NC) region, while persistent El Niño-like states were associated with a stronger WPSH and enhanced (diminished) precipitation in the JH (NC) region from ~1980 to 2000 CE<sup>24,28,43</sup> (Fig. S6).

**An 1800-year record of the tropical Pacific mean-state from East Asia.** As demonstrated by the close link between WPSH-dominated precipitation in East Asia and tropical Pacific mean-states, the tropical Pacific SST pattern dominates East Asian precipitation and its associated atmospheric circulation anomalies<sup>36–41,44</sup>. We therefore propose that precipitation records from the JH region and NC region, characterized by an antiphase response during the LIA and the MWP, are robust indicators of decadal-to-centennial changes in mean states. Considering their high temporal resolution and excellent age control (see Supplementary Table S1), we focus on the precipitation records from Lake Nvshan (in the JH region; blue star

in Fig. 1)<sup>41</sup> and Lake Gonghai (in the NC region; red star in Fig. 1)<sup>45</sup> to reconstruct an index of the tropical Pacific mean-state over the past 1800 years (Fig. 2). The reconstruction of JH region precipitation is based on sediment redness ( $a^*/L^*$  ratio)<sup>41</sup>. The sediment redness reflects sedimentary redox conditions that are sensitive to the changes of lake water level. Increased lake water levels cause reducing conditions and a blue-gray sediment color, while decreasing lake water level causes well-oxygenated conditions and red colored sediments<sup>41</sup>. As such, the sediment redness parameter ( $a^*/L^*$  ratio) indicates the precipitation-induced water level in Lake Nvshan, and thus can be used to reconstruct precipitation. The rainfall reconstruction from the NC region is based on pollen assemblages<sup>45</sup>. The pollen data were transformed into a proxy for annual precipitation based on the correlation between modern surface pollen distributions and precipitation<sup>45</sup>.

The reconstructed index of the tropical Pacific mean-state has four distinct centennial-scale phases over the past 1800 years (Figs. 2c and S7, see Supplementary Data). Negative Z-scores from 250 to 850 CE and 1050 to 1300 CE imply a more La Niña-like condition, whereas positive Z-scores from 950 to 1050 CE and 1400 to 1950 CE imply a more El Niño-like condition (Fig. 2c). The LIA was characterized by an El Niño-like state, and the MWP was characterized by La Niña-like state. To further confirm the reliability of our record we compared it to previous mean state reconstructions based on tropical Pacific SSTs<sup>9,14,46</sup>, tropical Pacific hydroclimate<sup>16</sup>, and Asian-Australian monsoon (AAM) region stalagmite  $\delta^{18}\text{O}$  Z-scores<sup>47</sup> over the past millennium, respectively (Fig. 3).

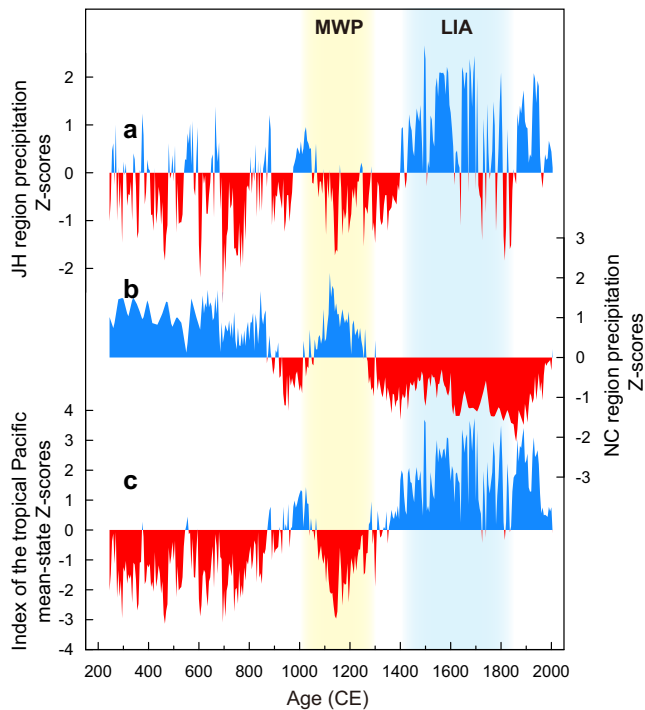


**Fig. 2** Index of the tropical Pacific mean-state reconstruction over the past 1800 years from precipitation anomalies in East Asia. **a** Normalized precipitation record based on sediments redness ( $a^*/L^*$  ratio) from Lake Nvshan, in the JH region of east-central China<sup>41</sup>, **b** normalized pollen-based precipitation reconstruction from Lake Gonghai in the NC region of northern China<sup>45</sup>, **c** index of the tropical Pacific mean-state as the difference between the reconstructed precipitation records from Lake Nvshan and Lake Gonghai. High precipitation and positive index are colored blue and low precipitation and negative index are colored red. The MWP period is shaded in yellow, and the LIA period is shaded in light blue.

The index of the tropical Pacific mean-state time series derived from lake sediments in the JH and NC regions of East Asia closely covaries with the time series of the zonal SST gradient in the tropical east-west Pacific<sup>46</sup> ( $r = -0.76$ ,  $p < 0.01$ ), the composite  $\delta^{18}\text{O}$  Z-scores of speleothems in the AAM region<sup>47</sup> ( $r = 0.42$ ,  $p < 0.05$ ), SST reconstructions in the central tropical North Pacific<sup>9</sup>, and zonal SST gradient in the equatorial Pacific<sup>14</sup>. Negative Z-scores of our index during the MWP that correspond with an increase in the zonal SST gradient across the tropical Pacific, a positive excursion in Northern Line Islands coral  $\delta^{18}\text{O}$  values, and a negative excursion in composite stalagmite  $\delta^{18}\text{O}$  Z-scores in the AAM region imply a La Niña-like condition during the MWP. Opposite conditions during the LIA conversely imply a persistent El Niño-like condition (Fig. 3a–d). Extratropical factors influencing the teleconnections between Pacific SST patterns and East Asian precipitation, such as the type of ENSO (Central Pacific (CP) type or Eastern Pacific (EP) type), have been proposed to influence the stationarity of teleconnections. However, the Coral  $\delta^{18}\text{O}$  (mean value) record from the central Pacific<sup>9</sup> and the SST reconstruction from the eastern Pacific<sup>11</sup> indicated that the CP ENSO and EP ENSO are covariable on the centennial timescale over the past millennium. We therefore propose that the index of the tropical Pacific mean-state reconstructed from East Asian precipitation records can be used to infer changes in the mean state of the tropical Pacific on centennial and longer time scales. This conclusion is supported by the observed covariation between the index of the tropical Pacific mean-state and the instrumental SOI from 1880 to 2005 CE on a decadal timescales (Fig. S8).

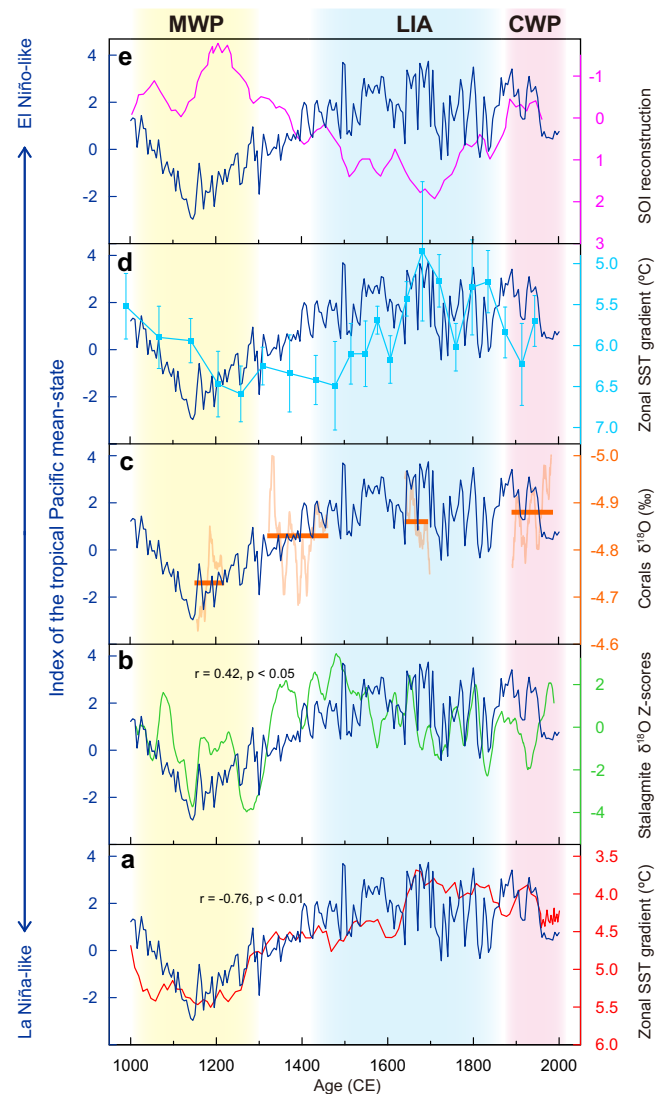


**Fig. 3** Comparison of the index of the tropical Pacific mean-state reconstructed from East Asian precipitation with other SST pattern reconstructions of the tropical Pacific. The index of the tropical Pacific mean-state from this study is plotted in each panel with a dark blue line. **a** Reconstructed zonal SST gradient across the tropical Pacific from the combined Indo Pacific Warm Pool (IPWP) and eastern equatorial Pacific (EEP) SST records<sup>46</sup> (red). **b** Composite stalagmite  $\delta^{18}\text{O}$  Z-scores in the Asian-Australian monsoon region<sup>47</sup> (green). **c** Coral  $\delta^{18}\text{O}$  values from Palmyra Island (6°N, 162°W) in the central tropical North Pacific<sup>9</sup> (orange). **d** Reconstructed zonal SST gradient across the tropical Pacific from the combined western Pacific warm pool (WPWP) and EEP SST records<sup>14</sup> (light blue). **e** Reconstructed SOI based on precipitation in the tropical Pacific<sup>16</sup> (pink). The yellow shading indicates the MWP, the blue shading indicates the LIA, and the red shading indicates the CWP.

However, the changes in mean state inferred from our record during the last millennium are opposite to those inferred from tropical Pacific Ocean hydroclimate variations<sup>16</sup> that indicate an El Niño-like pattern during the MWP and a La Niña-like pattern during the LIA (Fig. 3e). Changes in mean state inferred from SOI reconstructions are related to equatorial Pacific hydroclimate variations, and those inferred from our record are related to SST pattern variations. Hydrological changes in the equatorial Pacific are strongly modulated by both ENSO (which causes zonal changes) and the position of the ITCZ (which causes meridional changes), especially on centennial timescales<sup>21–23,48</sup>. Precipitation

variations in the Galápagos Islands (eastern equatorial Pacific) over the past millennium have been linked to the north-south movement of the ITCZ<sup>22</sup>, not just by ENSO. It is therefore possible that an SOI reconstruction based on hydrological climate variations in the equatorial Pacific are impacted by the ITCZ and ENSO (Fig. 3e) that are difficult to separate. What's more, changes in precipitation over the past millennium in the Galápagos Islands, which was used to reconstruct the SOI, are not always in agreement<sup>15,48</sup>. Galápagos precipitation reconstructed from paired hydrogen isotope ratios from microalgal and mangrove-derived sedimentary lipids in a coastal lake indicate a drier climate during the MWP and a wetter climate during the LIA<sup>48</sup>, whereas Galápagos precipitation reconstructed from sediment grain size in a high-elevation lake imply a wetter state during the MWP and a drier state during the LIA<sup>15</sup>. Furthermore, the ENSO record based on red color intensity from Lake Pallacocha sediments in the eastern tropical Pacific, has been reinterpreted as an unreliable ENSO indicator<sup>49</sup>. It is possible that these precipitation records were impacted by varying influences of SST pattern variations and ITCZ variations and that the discrepancies between the tropical Pacific mean-state reconstructions from SST and hydrological proxies in the equatorial Pacific may be due to interference from changes in the ITCZ and not just the SST pattern. Given the close covariation between the tropical Pacific mean-state reconstruction from East Asia and the mean state reconstructions from zonal SSTs in the tropical Pacific, coral  $\delta^{18}\text{O}$  in the Northern Line Islands, and composite stalagmite  $\delta^{18}\text{O}$  in the AAM region (Fig. 3a–d) that are not based on tropical Pacific hydroclimate directly as support for the veracity of the tropical Pacific mean-state reconstruction from East Asia. If that is the case then the MWP was La Niña-like and the LIA was El Niño-like.

**Possible forcing mechanisms of changes in the tropical Pacific mean-state over the past millennium.** The “ocean dynamical thermostat” mechanism, which favors the greater sensitivity of western equatorial Pacific (WEP) SSTs to radiative forcing relative to eastern equatorial Pacific (EEP) SSTs (less warming in the EEP compared with the WEP), has been invoked to explain the changes in the tropical Pacific mean-state over the past millennium<sup>50</sup>. Accordingly, increased radiative forcing across the equatorial Pacific (&/or globally) would drive the tropical Pacific into a La Niña-like state because it would warm the WEP more than the EEP and strengthen the Walker circulation<sup>50</sup>. Conversely, reduced radiative forcing would weaken the Walker circulation and drive the tropical Pacific toward an El Niño-like state<sup>50</sup>. Throughout the pre-industrial era our reconstructed mean state variations closely covary with total solar irradiance (TSI; Fig. 4d) ( $r = -0.61$ ,  $p < 0.01$ ) and effective radiative forcing<sup>52</sup> (Fig. 4c) ( $r = -0.52$ ,  $p < 0.05$ ), which includes both solar and volcanic forcing, in addition to global mean temperature<sup>52</sup> (GMT; Fig. 4a) ( $r = -0.75$ ,  $p < 0.01$ ), and northern hemisphere temperature<sup>53</sup> (NHT; Fig. 4b) ( $r = -0.59$ ,  $p < 0.01$ ). Negative Z-scores in our record, indicative of La Niña-like conditions, coincide with periods of high radiative forcing and GMT, such as during the MWP, while positive Z-scores, indicative of El Niño-like conditions, are concurrent with periods of lower radiative forcing and GMT, such as during the LIA (Fig. 4). The associations between greater radiative forcing, warmer GMT, and La Niña-like conditions during the MWP, and lower radiative forcing, colder GMT, and El Niño-like conditions during the LIA, are consistent with the “ocean dynamical thermostat” mechanism (Fig. 4)<sup>50</sup>, although other simulations argue that the response of tropical Pacific mean states to greater (lower) radiative forcing is an El Niño-like (La Niña-like) state<sup>54–56</sup>. The deeper thermocline

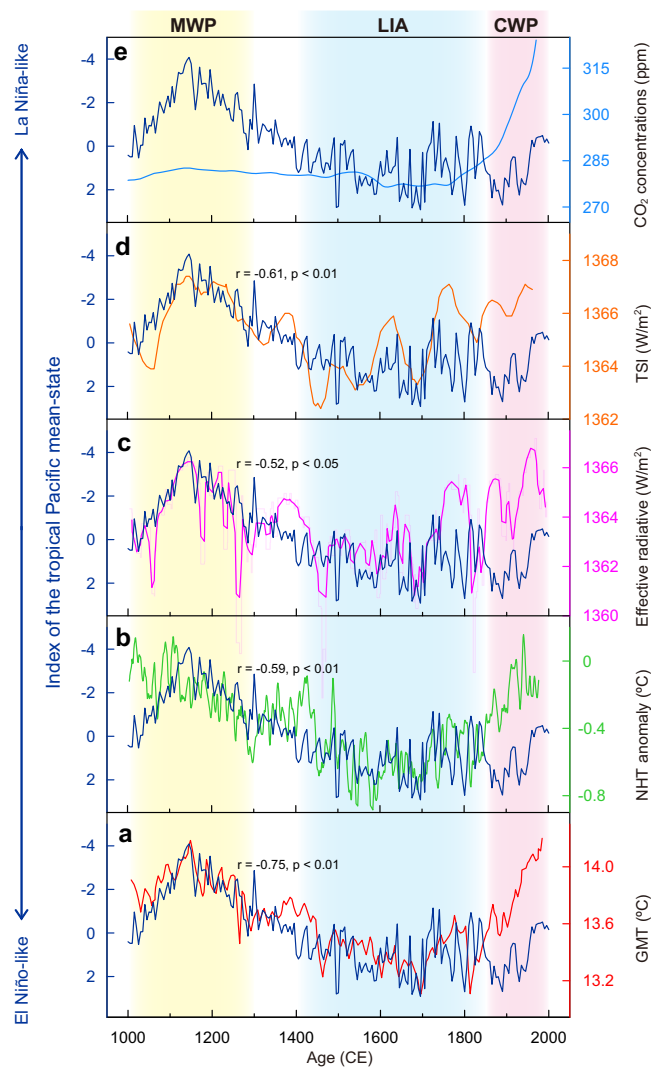


**Fig. 4 Comparison of the index of the tropical Pacific mean-state from East Asia with possible forcing mechanisms.** The index of the tropical Pacific mean-state reconstructed from East Asian lake sediments in this study is shown by the dark blue line in each panel. **a** Modeled global mean temperature (GMT) from an ECHO-G model simulation (red)<sup>52</sup>. **b** Northern Hemisphere temperature (NHT) reconstructions from proxy records (green)<sup>53</sup>. **c** Time series of effective radiative forcing integrated from global volcanic aerosols and solar irradiance (pink)<sup>52</sup>. **d** Total solar irradiance (TSI) derived from the common fluctuations in the production rates of the cosmogenic nuclides of  $^{14}\text{C}$  and  $^{10}\text{Be}$  production rates (orange)<sup>51</sup>. **e** Global  $\text{CO}_2$  concentration (light blue)<sup>70</sup>. Correlation coefficients and  $p$ -values between the index of the tropical Pacific mean-state and time series of forcing mechanisms during the pre-industrial era (1000–1850 CE) are shown in each panel. The yellow shading indicates the MWP, the blue shading indicates the LIA, and the red shading indicates the CWP.

in the WEP relative to the EEP, where upwelling causes shoaling of the thermocline, results in a greater sensitivity of WEP SSTs. During the MWP, when radiative forcing was higher (Fig. 4c, d), a larger zonal SST gradient characterized the tropical Pacific (Fig. 3a)<sup>50</sup>. This increased zonal SST gradient would have strengthened trade winds, cooled EEP SSTs via the upwelling of cold water, and further enhanced trade winds via the Bjerknes feedback. The resulting state of the tropical Pacific would have been La Niña-like during the MWP. The opposite situation, in which lower radiative forcing caused a reduced zonal SST

gradient would have resulted in an El Niño-like state during the LIA<sup>46,50</sup>.

However, the “ocean dynamical thermostat” mechanism is difficult to reconcile with more El Niño-like conditions during the CWP inferred from our record of the tropical Pacific mean-state and the zonal SST gradient in the tropical Pacific, since GMT continuously increased during this period (Fig. 4). Such an mean state during the CWP cannot be explained by the “ocean dynamical thermostat” mechanism, but is nevertheless consistent with some general circulation models (GCMs) that indicate a weakening of the Pacific Walker circulation, resulting in El Niño-like conditions, under global warming<sup>57,58</sup>. Warming increases the moist static energy in the atmosphere by a greater amount than the energy transports associated with precipitation. The increased moisture must be transported from the atmospheric boundary layer to the free troposphere, and this projects a weakening of Walker circulation and a weaker SST gradient (El Niño-like)<sup>57,58</sup>.

Differing impacts of radiative forcing caused by greenhouse gases and insolation on tropical Pacific climate have been observed in coupled ocean-atmosphere GCMs<sup>59</sup>. When warming is caused by increased greenhouse-gas forcing, the zonal SST gradient across the equatorial Pacific decreases, whereas when the warming is caused by increased effective radiation forcing, the zonal SST gradient increases<sup>52</sup>. Lacking any strong greenhouse gas forcing in the pre-industrial period (before ~1850 CE)<sup>52</sup> (Fig. 4e), we suggest that the “ocean dynamical thermostat” mechanism was responsible for the La Niña-like (El Niño-like) conditions during the MWP (LIA) when radiative forcing was enhanced by greater TSI and reduced volcanic aerosol loading of the atmosphere<sup>50</sup>. During the industrial period (post-1850; CWP), when increased greenhouse gas concentrations dominated the radiative forcing, the zonal SST gradient may have diminished, resulting in an El Niño-like state<sup>54–58</sup> (Fig. 4e), although studies to the contrary suggest that the rise in greenhouse gases corresponds to an enhanced zonal SST gradient (El Niño-like)<sup>59,60</sup>. Our reconstruction, together with some climate model simulations<sup>52,54–58</sup>, have implications for projecting future global changes when increased anthropogenic greenhouse gas forcing will promote a more El Niño-like state.

### Changes in variability and mean state of the tropical Pacific.

Our new tropical Pacific mean-state reconstruction allows assessment of the evolution of tropical Pacific SST pattern variability on centennial timescale under the La Niña-like state or El Niño-like state over the past millennium. Our record was processed using a 50-yr Lanczos high-pass filter, and then a 100-yr running biweight variance was calculated to infer tropical Pacific variability on centennial timescales (Fig. 5). Our variance record reveals large fluctuations on centennial timescales over the past millennium. The lowest variance (~0.25) occurred during the MWP. It then increased starting ~1400 CE and reached ~0.5 around 1500 CE. During the remainder of the LIA the variance decreased until 1600 CE (>0.25) before rising sharply to ~1.0 around 1650 CE and remaining high until the CWP. Overall, the centennial scale variance during the LIA and CWP was significantly higher than during the MWP. A spectral analysis<sup>61</sup> and wavelet transform<sup>62</sup> of the data clearly show a shift in periodicity between the MWP and the LIA, from a ~250 yr cycle to ~130 yr cycle (Fig. S9).

The changes in our tropical Pacific variability record are supported by other ENSO variance records spanning the last millennium, such as the North American Drought Atlas<sup>7</sup> ( $r = 0.78$ ,  $P < 0.05$ ) (Fig. 5b), the standard deviation of coral

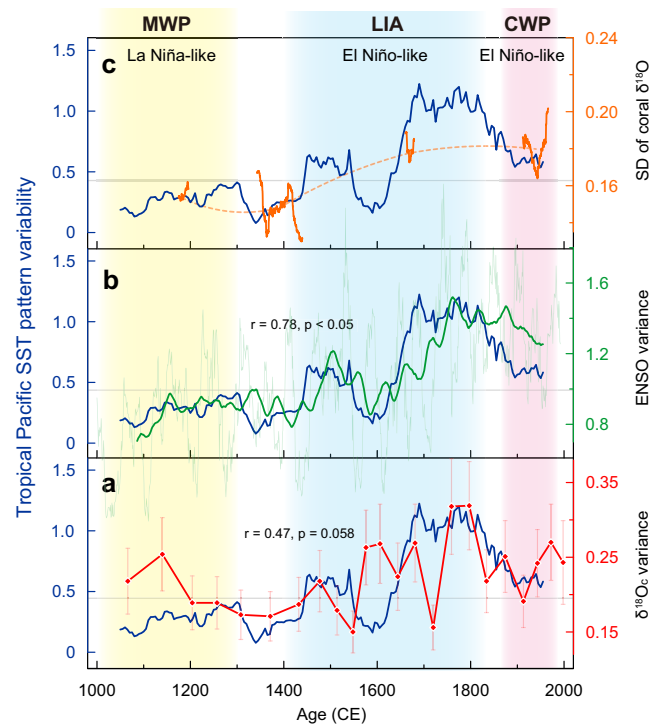


**Fig. 5 Comparison of records of the tropical Pacific variability.** The tropical Pacific SST pattern variance in this study is shown by the dark blue line in each panel. **a**  $\delta^{18}\text{O}$  variance from planktonic foraminifera in ocean sediment core KNR195-5 MC42C in the eastern equatorial Pacific (red)<sup>14</sup>. **b** ENSO variance record from the North American Drought Atlas (75-yr smoothing, green)<sup>7</sup>. **c** The standard deviation (SD, 50-yr sliding window, an indicator of variability on the interdecadal timescale) of coral  $\delta^{18}\text{O}$  values from Palmyra Island (orange)<sup>9</sup>. The yellow shading indicates the MWP, the blue shading indicates the LIA, and the red shading indicates the CWP.

$\delta^{18}\text{O}$  values at Palmyra Island<sup>9</sup> (Fig. 5c), and the  $\delta^{18}\text{O}$  variance of planktonic foraminifera from marine sediments in the eastern equatorial Pacific<sup>14</sup> ( $r = 0.47$ ,  $P = 0.058$ ) (Fig. 5a). Together, those records show broadly consistent changes: a lower variance during the MWP and a higher variance during the LIA and the CWP. As mentioned above, the MWP was characterized by a La Niña-like state, whereas the LIA and the CWP were characterized by El Niño-like states (Fig. 4). It is worth noting that the tropical Pacific variability and mean state generally correspond well on multi-centennial timescales. Tropical Pacific variability was greatly reduced under a La Niña-like state and increased under an El Niño-like state, which is supported by paleo-ENSO variance reconstructions<sup>7</sup> and model simulations<sup>3,4,63</sup>. This relationship may be explained by a positive feedback between ENSO variance and mean state<sup>3,4</sup>, whereby increasing ENSO variance causes an El Niño-like state, while an El Niño-like state in return amplifies ENSO variability. Therefore, like the changes in mean state, tropical Pacific variability also showed opposite responses during the MWP and the CWP.

### Conclusions

This study presents an 1800-yr reconstruction of the mean state of the tropical Pacific based on precipitation records derived from lake sediments in East Asia where rainfall is closely linked to SST anomalies via an atmospheric teleconnection. It indicates a La Niña-like state in the tropical Pacific with decreased variance during the MWP, and an El Niño-like state with increased variance during both the LIA and the post-1850 CE period.

These results confirm the different responses of the mean state of the tropical Pacific to global temperature changes before and after the industrial period derived from model simulations, and reconciles the difference between reconstructions of the mean state of the tropical Pacific based on SST and hydroclimate variations. Nonetheless, given the multiple drivers of hydroclimate proxies in the equatorial Pacific, additional high-resolution reconstructions from other ENSO-teleconnected regions would aid in understanding the forcing mechanisms causing long-term changes in the mean state of the tropical Pacific during the Common Era.

## Methods

**Precipitation records collection and classification.** To study the precipitation spatial pattern in East Asia during the LIA and the MWP, published paleo-precipitation records were collected based on the following criteria: (1) study sites must be located in East Asia and outside the direct influence of the ITCZ; (2) the chronology of each record was sufficient to identify the LIA and MWP periods; (3) the average temporal resolution was <70 years; 4) precipitation proxies applied are well accepted. In total, 20 records satisfied these criteria and were selected for consideration in this study (Supplementary Table S1).

The classification of dry-wet climate for each precipitation record during the LIA and the MWP is taken from previous study<sup>26</sup>. (1) The paleo-precipitation records were first linearly interpolated to their average resolution during the past millennium; (2) The Mi (median for each record) was calculated, in order to represent the normal level (indicated “moderate climate”) and avoid the influence of extreme values on the entire time series; (3) The interpolated values indicating a dry or wet climate during the MWP (LIA) were compared to the Mi (median for each record) of the entire time series, respectively. If 2/3 or more of the observations within the MWP (or LIA) period that were wetter than the median value (Mi) for the full record, the climate condition for that period was classified as “wet”. If 1/2–2/3 of the observations were wetter than Mi, the climate condition for that period was classified as “moderately wet”. If 2/3 or more of the observations within the MWP (or LIA) period that were dryer than the median value (Mi) for the full record, the climate condition for that period was classified as “dry”. If 1/2–2/3 of the observations were dryer than Mi, the climate condition for that period was classified as “moderately dry”.

**Construction of the index of the tropical Pacific mean-state.** The precipitation record reconstructed from Lake Nvshan (in JH region) has an average resolution of 1.4 years, and that from Lake Gonghai (in NC region) of 5.6 years. We first adjusted the two precipitation records to 5-year resolution using Acycle2.4.1<sup>64</sup>, and then normalized the interpolated precipitation records to the standard Z-score, and calculated the index of the tropical Pacific mean-state for the past millennium<sup>16</sup>:

$$Z = (X - V)/SD \quad (1)$$

where  $X$  is the original value,  $V$  and  $SD$  are the average and standard deviation of the time series, and  $Z$  is the normalized result.

Finally, the index of the tropical Pacific mean-state was constructed by subtracting the normalized NC region precipitation record from JH region precipitation record (Fig. 2):

$$Z_{(\text{index})} = Z_{\text{JH}} - Z_{\text{NC}} \quad (2)$$

where  $Z_{\text{JH}}$  and  $Z_{\text{NC}}$  are the normalized Z-scores of the precipitation from Lake Nvshan (in JH region) and Lake Gonghai (in NC region), respectively. Negative (positive) Z-scores represent more La Niña-like (El Niño-like) conditions over the past millennium.

Error estimations for the derived index of the tropical Pacific mean-state are provided in ref. <sup>16</sup>. The index of the tropical Pacific mean-state error arises from chronological uncertainties and proxy analytical uncertainties. The chronological uncertainties for the Lake Nvshan and Lake Gonghai records were obtained from the Bayesian age model software BACON in the R programming package<sup>65</sup> based on a 5 (Lake Nvshan) or 8 (Lake Gonghai) AMS <sup>14</sup>C dates on terrestrial plant residues<sup>41,45</sup>. The sediment redness measurements upon which the Lake Nvshan precipitation reconstruction is based had an analytical uncertainty of  $\pm 0.5\text{--}1\%$ <sup>41</sup>, while the uncertainty in reconstructed rainfall from the Lake Gonghai pollen record is  $\pm 88$  mm/yr<sup>45</sup>.

Monte Carlo simulations were used to determine the uncertainty of the index of the tropical Pacific mean-state. The simulation of dating uncertainties was based on the assumption that the effect of the dating uncertainty is roughly equivalent to temporally shifting the time series by the dating error. Then the minimum and maximum index values were calculated in the window of the dating error and assigned the index value to an evenly distributed random number between the minimum and maximum values. After application of this noise, both records were normalized to the standard Z-score; the difference between the two records was recalculated and denoted as the index of the tropical Pacific mean-state (see “Methods” above). The Monte Carlo simulation was repeated 1000 times, resulting in 1000 records of the tropical Pacific mean-state, from which the standard

deviation was calculated for each age point. This uncertainty of the index is presented as the standard deviation confidence intervals (Fig. S7).

**Statistical significance test.** The Pearson correlation coefficient  $r$  is used to test the correlation of two time series  $A$  and  $B$ , using the equation:

$$r = \frac{\sum_{k=1}^n (a_k - a_m)(b_k - b_m)}{(n-1)s_a s_b} \quad (3)$$

where  $n$  is the number of samples of the time series  $A$  and  $B$ ,  $a_m$  and  $b_m$  are the sample means of  $A$  and  $B$ , and  $s_a$  and  $s_b$  are the sample standard deviations of  $A$  and  $B$ .

The lower degree of freedom associated with relatively short length and auto-correlations between the two-time series also must be considered based on the effective number of independent values<sup>66</sup>. Firstly, DT (the time between independent values) was calculated using the equation<sup>67,68</sup>:

$$DT = \frac{1 + r_a r_b}{1 - r_a r_b} \quad (4)$$

where  $r_a$  and  $r_b$  are the lag-1 series correlation of the time series  $A$  and  $B$ .

Then,  $N_{\text{eff}}$  (the effective number of independent values) was calculated from the equation:

$$N_{\text{eff}} = n/DT \quad (5)$$

Finally, the  $P$ -value corresponding to  $N_{\text{eff}}$  (see Supplementary Table S2) according to the significance correlation coefficient test table<sup>69</sup>.

**Reporting summary.** Further information on research design is available in the Nature Portfolio Reporting Summary linked to this article.

## Data availability

The data for the index of the tropical Pacific mean-state are available online for download at figshare (<https://doi.org/10.6084/m9.figshare.22140608>).

Received: 6 September 2022; Accepted: 24 February 2023;  
Published online: 15 March 2023

## References

- Wang, C. Atmospheric circulation cells associated with the El Niño–Southern Oscillation. *J. Clim.* **15**, 399–419 (2002).
- Tsonis, A. A., Hunt, A. G. & Elsner, J. B. On the relation between ENSO and global climate change. *Meteorol. Atmos. Phys.* **84**, 229–242 (2003).
- McPhaden, M. J., Zebiak, S. E. & Glantz, M. H. ENSO as an integrating concept in earth science. *Science* **314**, 1740–1745 (2006).
- Yeh, S. W. & Kirtman, B. P. ENSO amplitude changes due to climate change projections in different coupled models. *J. Clim.* **20**, 203–217 (2007).
- Choi, J., An, S.-I., DeWitte, B. & Hsieh, W. W. Interactive feedback between the tropical Pacific Decadal Oscillation and ENSO in a coupled general circulation model. *J. Clim.* **22**, 6597–6611 (2009).
- Fedorov, A. V. & Philander, S. G. A stability analysis of tropical ocean–atmosphere interactions: Bridging measurements and theory for El Niño. *J. Clim.* **14**, 3086–3101 (2001).
- Li, J. et al. Interdecadal modulation of El Niño amplitude during the past millennium. *Nat. Clim. Change* **1**, 114–118 (2011).
- Cai, W. et al. Changing El Niño–Southern Oscillation in a warming climate. *Nat. Rev. Earth Environ.* **2**, 628–644 (2021).
- Cobb, K. M., Charles, C. D., Cheng, H. & Edwards, R. L. El Niño/Southern Oscillation and tropical Pacific climate during the last millennium. *Nature* **424**, 271–276 (2003).
- Cobb, K. M. et al. Highly variable El Niño–southern oscillation throughout the Holocene. *Science* **339**, 67–70 (2013).
- Conroy, J. L. et al. Unprecedented recent warming of surface temperatures in the eastern tropical Pacific Ocean. *Nat. Geosci.* **2**, 46–50 (2009).
- Mann, M. E. et al. Global signatures and dynamical origins of the Little Ice Age and Medieval Climate Anomaly. *Science* **326**, 1256–1260 (2009).
- Dee, S. G. et al. No consistent ENSO response to volcanic forcing over the last millennium. *Science* **367**, 1477–1481 (2020).
- Rustic, G. T., Koutavas, A., Marchitto, T. M. & Linsley, B. K. Dynamical excitation of the tropical Pacific Ocean and ENSO variability by Little Ice Age cooling. *Science* **350**, 1537–1541 (2015).
- Conroy, J. L., Overpeck, J. T., Cole, J. E., Shanahan, T. M. & Steinitz-Kannan, M. Holocene changes in eastern tropical Pacific climate inferred from a Galápagos lake sediment record. *Quat. Sci. Rev.* **27**, 1166–1180 (2008).
- Yan, H. et al. A record of the Southern Oscillation Index for the past 2,000 years from precipitation proxies. *Nat. Geosci.* **4**, 611–614 (2011).

17. Chiang, J. C. H., Zebiak, S. E. & Cane, M. A. Relative roles of elevated heating and surface temperature gradients in driving anomalous surface winds over tropical oceans. *J. Atmos. Sci.* **58**, 1371–1394 (2001).
18. Oppo, D. W., Rosenthal, Y. & Linsley, B. K. 2,000-year-long temperature and hydrology reconstructions from the Indo-Pacific warm pool. *Nature* **460**, 1113–1116 (2009).
19. Mann, M. E., Cane, M. A., Zebiak, S. E. & Clement, A. Volcanic and solar forcing of the tropical Pacific over the past 1000 years. *J. Clim.* **18**, 447–456 (2005).
20. Man, W. & Zhou, T. Forced response of atmospheric oscillations during the last millennium simulated by a climate system model. *Chin. Sci. Bull.* **56**, 3042–3052 (2011).
21. Newton, A., Thunell, R. & Stott, L. Climate and hydrographic variability in the Indo-Pacific Warm Pool during the last millennium. *Geophys. Res. Lett.* **33**, L19710 (2006).
22. Sachs, J. P. et al. Southward movement of the Pacific intertropical convergence zone AD 1400–1850. *Nat. Geosci.* **2**, 519–525 (2009).
23. Richey, J. N. & Sachs, J. P. Precipitation changes in the western tropical Pacific over the past millennium. *Geology* **44**, 671–674 (2016).
24. Ding, Y., Sun, Y., Wang, Z., Zhu, Y. & Song, Y. Inter-decadal variation of the summer precipitation in China and its association with decreasing Asian summer monsoon Part II: Possible causes. *Int. J. Climatol.* **29**, 1926–1944 (2009).
25. Jing, T., Zhang, Q., Zhu, D. & Wu, Y. W. Yangtze floods and droughts (China) and teleconnections with ENSO activities (1470–2003). *Quat. Int.* **144**, 29–37 (2006).
26. Chen, J. et al. Hydroclimatic changes in China and surroundings during the Medieval Climate Anomaly and Little Ice Age: spatial patterns and possible mechanisms. *Quat. Sci. Rev.* **107**, 98–111 (2015).
27. Liu, H. et al. A 13,000-year peatland palaeohydrological response to the ENSO-related Asian monsoon precipitation changes in the middle Yangtze Valley. *Quat. Sci. Rev.* **212**, 80–91 (2019).
28. Liu, J. et al. Dipolar mode of precipitation changes between North China and the Yangtze River valley existed over the entire Holocene: evidence from the sediment record of Nanyi Lake. *Int. J. Climatol.* **41**, 1667–1681 (2021).
29. Mann, M. E. *Little Ice Age, Encyclopedia of Global Environmental Change* 504–509 (Wiley Press, 2002).
30. Wilson, R. et al. Last millennium Northern Hemisphere summer temperatures from tree rings: Part I: the long term context. *Quat. Sci. Rev.* **134**, 1–18 (2016).
31. Bard, E., Raisbeck, G., Yiou, F. & Jouzel, J. Solar irradiance during the last 1200 years based on cosmogenic nuclides. *Tellus Ser. B Chem. Phys. Meteorol.* **52**, 985–992 (2000).
32. Gao, C., Robock, A. & Ammann, C. Volcanic forcing of climate over the past 1500 years: an improved ice core-based index for climate models. *J. Geophys. Res.: Atmospheres* **113**, 1984–2012 (2008).
33. Atwood, A. R., Wu, E., Frierson, D. M. W., Battisti, D. S. & Sachs, J. P. Quantifying climate forcings and feedbacks over the last millennium in the CIMP5-PMIP3 models. *J. Clim.* **29**, 1161–1178 (2016).
34. Atwood, A. R., Battisti, D. S., Wu, E., Frierson, D. M. W. & Sachs, J. P. Data-model comparisons of tropical hydroclimate changes over the common era. *Paleoceanogr. Paleoclimatol.* **36**, e2020PA003934 (2021).
35. Cook, E. R., Seager, R., Cane, M. A. & Stahle, D. W. North American drought: reconstructions, causes, and consequences. *Earth-Sci. Rev.* **81**, 93–134 (2007).
36. Seager, R. et al. Blueprints for medieval hydroclimate. *Quat. Sci. Rev.* **26**, 2322–2336 (2007).
37. Graham, N., Ammann, C., Fleitmann, D., Cobb, K. & Luterbacher, J. Support for global climate reorganization during the “Medieval climate anomaly”. *Clim. Dyn.* **37**, 1217–1245 (2011).
38. Yu, L., Furevik, T., Ottera, O. H. & Gao, Y. Modulation of the Pacific Decadal Oscillation on the summer precipitation over East China: a comparison of observations to 600-years control run of Bergen Climate Model. *Clim. Dyn.* **44**, 475–494 (2015).
39. Yang, Q. et al. Decadal modulation of precipitation patterns over Eastern China by sea surface temperature anomalies. *J. Clim.* **30**, 7017–7033 (2017).
40. Ye, T., Shen, Q., Wang, K., Zhang, Z. & Zhao, J. Interdecadal change of the northward jump time of the western Pacific subtropical high in association with the Pacific decadal oscillation. *J. Meteorol. Res.* **29**, 59–71 (2015).
41. Jiang, S. et al. Central eastern China hydrological changes and ENSO-like variability over the past 1800 yr. *Geology* **49**, 1386–1390 (2021).
42. Liu, Z. et al. Evolution and forcing mechanisms of El Niño over the past 21,000 years. *Nature* **515**, 550–553 (2014).
43. Li, H., Dai, A., Zhou, T. & Lu, J. Responses of East Asian summer monsoon to historical SST and atmospheric forcing during 1950–2000. *Clim. Dyn.* **34**, 501–514 (2010).
44. Zhang, Q., Zheng, Y., Singh, V. P., Luo, M. & Xie, Z. Summer extreme precipitation in eastern China: mechanisms and impacts. *J. Geophys. Res.-Atmos.* **122**, 2766–2778 (2017).
45. Chen, F. et al. East Asian summer monsoon precipitation variability since the last deglaciation. *Sci. Rep.* **5**, 1–11 (2015).
46. Conroy, J. L., Overpeck, J. T. & Cole, J. E. El Niño/Southern Oscillation and changes in the zonal gradient of tropical Pacific sea surface temperature over the last 1.2 ka. *PAGES news* **18**, 32–34 (2010).
47. Zhang, J. et al. Asian-Australian monsoon evolution over the last millennium linked to ENSO in composite stalagmite  $\delta^{18}\text{O}$  records. *Quat. Sci. Rev.* **281**, 107420 (2022).
48. Nelson, D. B. & Sachs, J. P. Galápagos hydroclimate of the Common Era from paired microalgal and mangrove biomarker  $^2\text{H}/^1\text{H}$  values. *Proc. Natl. Acad. Sci. USA* **113**, 3476–3481 (2016).
49. Schneider, T., Hampel, H., Mosquera, P. V., Tylmann, W. & Grosjean, M. Paleo-ENSO revisited: Ecuadorian Lake Pallacocha does not reveal a conclusive El Niño signal. *Glo. Plane. Change* **168**, 54–66 (2018).
50. Clement, A. C., Seager, R., Cane, M. A. & Zebiak, S. E. An ocean dynamical thermostat. *J. Clim.* **9**, 2190–2196 (1996).
51. Bard, E. Nuclide production by cosmic rays during the Last Ice Age. *Science* **277**, 532–533 (1997).
52. Liu, J., Wang, B., Cane, M. A., Yim, S. Y. & Lee, J. Y. Divergent global precipitation changes induced by natural versus anthropogenic forcing. *Nature* **493**, 656–659 (2013).
53. Mann, M. E. & Jones, P. D. Global surface temperatures over the past two millennia. *Geophys. Res. Lett.* **30**, 1820 (2003).
54. Knutson, T. R. & Manabe, S. Time-mean response over the tropical Pacific to increased  $\text{CO}_2$  in a coupled ocean-atmosphere model. *J. Clim.* **8**, 2181–2199 (1995).
55. Liu, Z., Vavrus, S., He, F., Wen, N. & Zhong, Y. Rethinking tropical ocean response to global warming: the enhanced equatorial warming. *J. Clim.* **18**, 4684–4700 (2005).
56. Xie, S. et al. Global warming pattern formation: sea surface temperature and rainfall. *J. Clim.* **23**, 966–986 (2010).
57. Vecchi, G. A. et al. Weakening of tropical Pacific atmospheric circulation due to anthropogenic forcing. *Nature* **441**, 73–76 (2006).
58. Held, I. & Soden, B. Robust responses of the hydrological cycle to global warming. *J. Clim.* **19**, 5686–5699 (2006).
59. Cane, M. A. et al. Twentieth century sea surface temperature trends. *Science* **275**, 957–960 (1997).
60. Seager, R. et al. Strengthening tropical Pacific zonal sea surface temperature gradient consistent with rising greenhouse gases. *Nat. Clim. Change* **9**, 517–522 (2019).
61. Mann, M. E. & Lees, J. Robust estimation of background noise and signal detection in climatic time series. *Clim. Change* **33**, 409–445 (1996).
62. Torrence, C. & Compo, G. P. A practical guide to wavelet analysis. *Bull. Am. Meteorol. Soc.* **79**, 61–78 (1998).
63. Karnauskas, K. B., Smerdon, J. E., Seager, R. & González-Rouco, J. F. A Pacific centennial oscillation predicted by coupled GCMs. *J. Clim.* **25**, 5943–5961 (2012).
64. Li, M., Hinnov, L. & Kump, L. Acycle: time-series analysis software for paleoclimate research and education. *Comput. Geotech.* **127**, 12–22 (2019).
65. Blaauw, M. & Christen, J. A. Flexible paleoclimate age-depth models using an autoregressive gamma process. *Bayesian Anal.* **6**, 457–474 (2011).
66. Davis, R. E. Techniques for statistical analysis and prediction of geophysical fluid systems. *Geophys. Astrophys. Fluid Dyn.* **8**, 245–277 (1977).
67. Bretherton, C. S., Widmann, M., Dymnikov, V. P., Wallace, J. M. & Blade, I. The effective number of spatial degrees of freedom of a time-varying field. *J. Clim.* **12**, 1990–2009 (1999).
68. Wang, J. et al. Internal and external forcing of multidecadal Atlantic climate variability over the past 1200 years. *Nat. Geosci.* **10**, 512–517 (2017).
69. Huang, J. *Meteorological Statistical Analysis and Forecast Method (Third Edition)* (Meteorology Press, 2007).
70. Frank, D. C. et al. Ensemble reconstruction constraints on the global carbon cycle sensitivity to climate. *Nature* **463**, 527–530 (2010).

## Acknowledgements

This study is jointly supported by the National Natural Science Foundation of China (grants 41888101, 41721002), Strategic Priority Research Program of the Chinese Academy of Sciences (grant XDB26000000), China Postdoctoral Science Foundation (grant 2022M713024), CAS Youth Interdisciplinary Team (grant JCTD-2021-05), and the Youth Innovation Promotion Association CAS (grant 2018498). We are grateful for the helpful discussions with Qing Yan, Fei Liu, Jianqiu Zheng, and Hongjing Niu.

## Author contributions

X.Z. and S.J. designed the study. S.J. and X.Z. wrote the paper. S.J., X.Z., J.P.S., and Y.S. contributed to the discussion of results and manuscript refinement. S.J., Z.L. Y.L., X.L., and A. C. analyzed the data. L.T. and J.P.S. contributed to improving the English. All authors discussed the results and implications and commented on the manuscript at all stages.

## Competing interests

The authors declare no competing interests.

**Additional information**

**Supplementary information** The online version contains supplementary material available at <https://doi.org/10.1038/s43247-023-00734-4>.

**Correspondence** and requests for materials should be addressed to Xin Zhou.

**Peer review information** *Communications Earth & Environment* thanks the anonymous reviewers for their contribution to the peer review of this work. Primary Handling Editor: Aliénor Lavergne. Peer reviewer reports are available.

**Reprints and permission information** is available at <http://www.nature.com/reprints>

**Publisher's note** Springer Nature remains neutral with regard to jurisdictional claims in published maps and institutional affiliations.



**Open Access** This article is licensed under a Creative Commons Attribution 4.0 International License, which permits use, sharing, adaptation, distribution and reproduction in any medium or format, as long as you give appropriate credit to the original author(s) and the source, provide a link to the Creative Commons license, and indicate if changes were made. The images or other third party material in this article are included in the article's Creative Commons license, unless indicated otherwise in a credit line to the material. If material is not included in the article's Creative Commons license and your intended use is not permitted by statutory regulation or exceeds the permitted use, you will need to obtain permission directly from the copyright holder. To view a copy of this license, visit <http://creativecommons.org/licenses/by/4.0/>.

© The Author(s) 2023, corrected publication 2023